Ex vivo mechanical properties of human thoracolumbar fascia and erector spinae aponeurosis under traction loading and shear wave elastography

Maud Creze, Alexandre Lagache, Fabrice Duparc, Mila Broqué, Sylvain Persohn, Camille Slama, Claudio Vergari, Pierre-Yves Rohan

Journal of the Mechanical Behavior of Biomedical Materials 168 (2025) 107028

Contents lists available at ScienceDirect

Journal of the Mechanical Behavior of Biomedical Materials

journal homepage: www.elsevier.com/locate/jmbbm

Ex vivo mechanical properties of human thoracolumbar fascia and erector spinae aponeurosis under traction loading and shear wave elastography

Maud Creze [a,b,c,*], Alexandre Lagache [a], Fabrice Duparc [d], Mila Broqué [a], Sylvain Persohn [a], Camille Slama [a], Claudio Vergari [a], Pierre-Yves Rohan [a]

[a] Arts et Métier Institute of Technology, Institut de Biomécanique Humaine Georges Charpak, Université Sorbonne Paris Nord, Paris, France
[b] Radiology Department, Bicêtre Hospital, DMU SMART IMAGING, Assistance Publique des Hôpitaux de Paris, Le Kremlin Bicêtre, France
[c] BIOMAPS, Université Paris-Saclay, Orsay, France
[d] Laboratory of Anatomy, Faculty of Medicine, Rouen-Normandy University, Rouen, France

ARTICLE INFO

Keywords:
Lumbar fascia
Back muscles
Materials testing
Shear waves elastography
Anisotropy

ABSTRACT

The thoracolumbar fascia (TLF) and the erector spinae aponeurosis (ESA) play an important role in the biomechanics of the spine and could be a source of low back pain. Although the TLF and ESA are key structures in several musculoskeletal dysfunctions and in tissue engineering, there is still a lack of evidence in the literature to prove that they have different mechanical properties and roles when considered as a single tissue. Furthermore, no methods are currently available to study these structures *in vivo*. The objective of this study was to analyze the ex-vivo tensile properties TLF and ESA, and to test the potential of ultrasound shearwave elastography (SWE) to characterize these tissues. Hundred samples from N = 10 fresh-frozen human donors were studied. Shear wave speed (SWS) was measured in all samples with SWE, and their tensile properties were measured with mechanical testing. Results show that TLF is anisotropic, and more compliant than ESA. SWS was not significantly correlated to tensile moduli.

These findings could potentially aid surgeons in their daily practices, assist engineers with in silico simulations, and support physiotherapists in musculoskeletal rehabilitation by enabling them to customize medical interventions for each specific patient and clinical condition. However, further research is necessary to further investigate the behavior in terms of time-dependent response and link between the tissue anisotropy and microstructural organization.

1. Introduction

The back fasciae and aponeurosis appear to play a major role in the stability of the lumbar spine and in the transmission of myofascial load to or from the limbs (Barker et al., 2004; Gracovetsky et al., 1981; Vleeming et al., 1995). They dissipate and sustain excessive load, transmit forces generated by the contraction of skeletal muscles and provide proprioceptive and nociceptive transduction (Barker et al., 2006). They are composed of two main tissues that are anatomically and functionally superimposed: the ThoracoLumbar Fascia (TLF) on the superficial layer and the Erector Spinae Aponeurosis (ESA) on the deep layer (Creze et al., 2018; Sato et al., 2021; Willard et al., 2012) The TLF serves as the insertion aponeurosis of several muscles including the latissimus dorsi muscle and the transversus abdominis muscle (Macintosh et al., 1987) while the ESA serves as both the distal tendon of the erector spinae muscles and the insertion aponeurosis of its muscle fibers (Bustami, 1986). These tissues are therefore reinforced by collagen fibers that are oriented in the direction of the main loading.

It is becoming increasingly clear that their damage is involved in spinal dysfunction and contributes to the pathogenesis of various back disorders, including low back pain (Casato et al., 2019; Langevin, 2011; Langevin et al., 2009; McGill, 1987; Wilke et al., 2017). Studies have shown that changes in morphology and material properties are responsible for back diseases, such as low back pain. In a study using ultrasound imaging, Langevin et al. (Langevin, 2011; Langevin et al., 2009) observed an increase in the thickness of the TLF and a reduction in shearing motion in patients with chronic low back pain. Similarly, Chen et al., 2020, 2021 and Tamartash et al. (2023) demonstrated variations in *vivo* stiffness, as assessed using shear wave elastography (SWE), during different postures in people with low back pain. Spinal surgery

* Corresponding author.78 rue du General Bicêtre, Le Kremlin Bicêtre, 94270, France
E-mail address: Maud.creze@aphp.fr (M. Creze).

https://doi.org/10.1016/j.jmbbm.2025.107028
Received 18 November 2024; Received in revised form 14 April 2025; Accepted 19 April 2025
Available online 19 April 2025

altered the tensile properties of the TLF, which had consequences on the overall spinal function (Nelson-Wong et al., 2018).

However, there is limited knowledge regarding the material properties of the back fasciae and aponeurosis. Evaluating material properties *in vivo* poses a significant challenge in mechanics research due to the difficulty of measuring morphology and force (Bojairami et al., 2022; Hukins et al., 1990). Thus, *ex vivo* materials testing of excised tissue samples under carefully controlled experimental environments are the current gold standard for material property estimation, despite the fact that these approaches remove the tissue from the native mechanical environment.

Several studies have investigated the mechanical properties of fascia and aponeurosis. For instance, Stecco et al. (2014), Bonaldi et al. (2023) and Otsuka et al. (2018) studied the thigh fascia lata, Kirilova et al. (2011) investigated the human abdominal fascia, while Natali et al., 2010. (Natali et al., 2010), Quian et al. (Qian et al., 2021) and Stecco et al. (2014) focused on the plantar fascia. These studies have shown that fascia and aponeurosis have properties common to biological soft tissues such as anisotropy, nonlinearity, viscoelasticity, and heterogeneity. However, to the best of the authors' knowledge, only the Yahia group (Yahia et al., 1993) has focused on the mechanical characterization of human TLF, and no studies have been conducted on the ESA. This study has revealed the presence of tissue strain-stiffening effects inducing a non-linear elastic behavior and resulting in an apparent elastic modulus increase as a function of the local tissue strain. This was confirmed in animal models, specifically murine and porcine TLF (Schleip et al., 2012).

Quantitative ultrasound elastography is beginning to emerge as a promising diagnostic tool for evaluating the mechanical properties of soft tissues *in vivo* (Bercoff et al., 2004; Gennisson et al., 2013). This technique has been widely used in clinics for various purposes, such as staging liver fibrosis (Ferraioli et al., 2012; Friedrich-Rust et al., 2008) assessing breast mass (Berg et al., 2012; Chang et al., 2011), and differentiating the properties of thyroid nodules (Lin et al., 2014; Sebag et al., 2010). In musculoskeletal research, the mechanical behavior of skeletal muscle *in vivo* (Ranger et al., 2024; Xu et al., 2023; Yoshitake et al., 2014; Dorado Cortez et al., 2016) and of the tensor fasciae latae *in vivo* (Chen et al., 2020, 2021; Tamartash et al., 2023) has been characterized using the Shearwave Imaging (SSI) technique. SWE has also demonstrated stiffness changes during various postures and with low back pain (Chen et al., 2020, 2021; Tamartash et al., 2023). However, the fundamental assumptions that allow shear wave propagation to be related to initial shear modulus—namely linearity, purely elastic behavior, homogeneity, and quasi-incompressibility—hold true for homogeneous isotropic soft tissues such as liver and breast tissues, but are not applicable to anisotropic and inhomogeneous tissues such as the thoracolumbar fascia (TLF) and erector spinae aponeurosis (ESA) and skeletal muscles. To ensure that investigators obtain robust and meaningful results baseline reliability and validity assessment are necessary.

Previous studies have investigated the correlation between SWE-derived stiffness and traditional mechanical testing techniques. Eby et al. (2013) reported a significant positive correlation between SWE-derived stiffness and traditional materials testing techniques derived stiffness. Likewise, in human cadaveric Achilles tendon (Haen et al., 2017) showed that there was a significant correlation ($R^2 = 0.95$) between shear moduli (SWE) and apparent elastic moduli (tensile tests). Similar results were reported by (Brandão et al., 2023) (i.e. a strong significant positive correlation between SSI-measured shear elastic modulus and tangent in human Achilles ($R = 0.97–0.99$) and patellar tendons ($R = 0.87–0.97$). To the best of the authors' knowledge, no studies have been conducted on thin structures such as the ESA. Recent studies on the biomechanical characterization of anisotropic tissues highlight that stiffness measurements using SWE do not necessarily reflect tensile properties. Gotschi et al. (Götschi et al., 2023) showed that shear wave propagation velocity is mainly influenced by shear viscoelastic properties rather than tensile stiffness, questioning the applicability of SWE for estimating Stiffness in highly structured tissues such as fascia. Additionally, the assessment of fascial tissues using SWE is complicated by wave-guiding effects and the geometric constraints of thin samples.

The objective of this study was to analyze the biomechanical tensile properties of *ex vivo* thoracolumbar fascia (TLF) and erector spinae aponeurosis (ESA) obtained from 10 fresh-frozen human donors using uniaxial tensile tests. Which form the primary contribution of this work. This analysis aimed to identify structural differences between these tissues and establish baseline mechanical properties. Additionally, SWE was explored as a complementary, non-invasive technique for assessing local shear properties *in vivo*. To do so, we measured the shear elastic modulus using the SSI technique and compared it with the tangent modulus obtained from mechanical tensile testing. Given the independent nature of shear and tensile moduli in anisotropic tissues, our goal was not to establish a direct correlation but rather to evaluate the potential of SWE as a supplementary tool in fascial biomechanics research.

2. Material and methods

Fig. 1 below provides an overview of the proposed methodology.

2.1. Human sample collection

All tests and procedures were conducted in accordance with French ethical rules and laws governing experiments involving post-mortem human subjects. Back fascia and aponeurosis were harvested from **ten adult donors** (mean age 91, range: 83–99 years; 7 females) at the School of Surgery (Assistance Publique des Hôpitaux de Paris, APHP) and the Anatomy department of Rouen-Normandy University. None of the donors showed any macroscopically visible damage to the lumbar back region, including surgical interventions, scoliosis, or traumatic lesions of the thoracolumbar region. The paraspinal muscles, paravertebral aponeurosis, thoracolumbar fascia, and subcutaneous adipose tissue were removed *en bloc* two to five days after death and stored at −41 °C.

2.2. Sample preparation

Tissue blocks were thawed one day prior to mechanical testing. This was achieved by slowly thawing them in the refrigerator for 18 h, followed by leaving them at room temperature (24 °C) for 3 h. The TLF and the ESA were then carefully dissected from the overlying adipose tissue and underlying muscle, respectively. A blunt dissection technique was used to separate the ESA and the TLF (as shown in Fig. 1). The samples were classified into four distinct groups as recalled in Fig. 1: Cranial ESA (ESA harvested from top positions), caudal ESA (ESA harvested from bottom positions), TLF (TLF harvested from bottom positions) and vertebral aponeurosis (VA) (TLF harvested from top positions).

To prevent tissue damage to the sample, a small amount of residual muscle or loose connective tissue was left on each sample. Two to three test samples of 70–100 mm in length and 10–20 mm in width were cut using a razor on a cutting board from each tissue. The samples for the ESA were oriented according to the direction of the main collagen fibers, which roughly corresponds to the longitudinal axis of the spine (cranio-caudal) (as shown in Fig. 2(b)). Samples from the Erector Spinae Aponeurosis (ESA) were divided into two groups based on their cranial or caudal location (close to the transition with the tendon) (as illustrated in Fig. 2(b)). The thoracolumbar fascia (TLF) was also divided into two sample types: a caudal sample, where the fascia has fibers with different orientations (TLF), and a cranial sample, where the fibers are oblique, upward, and outward defined as the vertebral aponeurosis (VA) (as shown in Fig. 2(c)). As the caudal sample had fibers without main orientation, it was cut according to the longitudinal axis of the spine by analogy with the ESA sample. The cranial sample was oriented oblique, upward, and outward like its constituent fibres. To prevent dehydration,

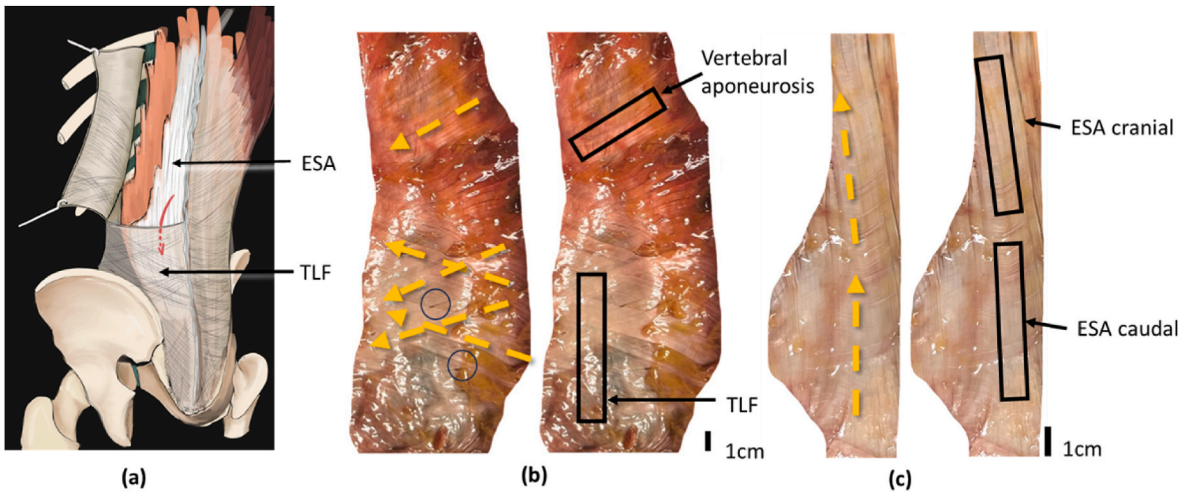

Fig. 1. Classification of the tissue samples based on the tissue type and location. (a) Posterior view of the back. The red arrows shows the cleavage plane between the ESA and the TLF. (b) Deep face of the TLF classified into TLF and vertebral aponeurosis (VA). Blue circles correspond to defects in the tissue allowing for the passage of vessels and nerves. (c) Superficial face of the ESA classified into cranial ESA (ESA harvested from top positions) and caudal ESA (ESA harvested from bottom positions). The superimposed black rectangles correspond to the location of the sample taken from the TLF and ESA. Yellow dashed arrows show mains fiber orientation in the tissues. The superimposed black rectangles indicate the sample extraction sites for TLF and ESA. Yellow dashed arrows represent the primary fiber orientations within the tissues. For TLF tensile testing, samples were taken perpendicular to the predominant fiber orientation (cross-fiber direction). This approach allowed for evaluating the mechanical behavior across the primary collagen fiber alignment rather than along it. The samples were clamped carefully to ensure uniform loading and minimize edge effects during testing. These considerations were essential to accurately assess the anisotropic mechanical response of the TLF. (For interpretation of the references to color in this figure legend, the reader is referred to the Web version of this article.)

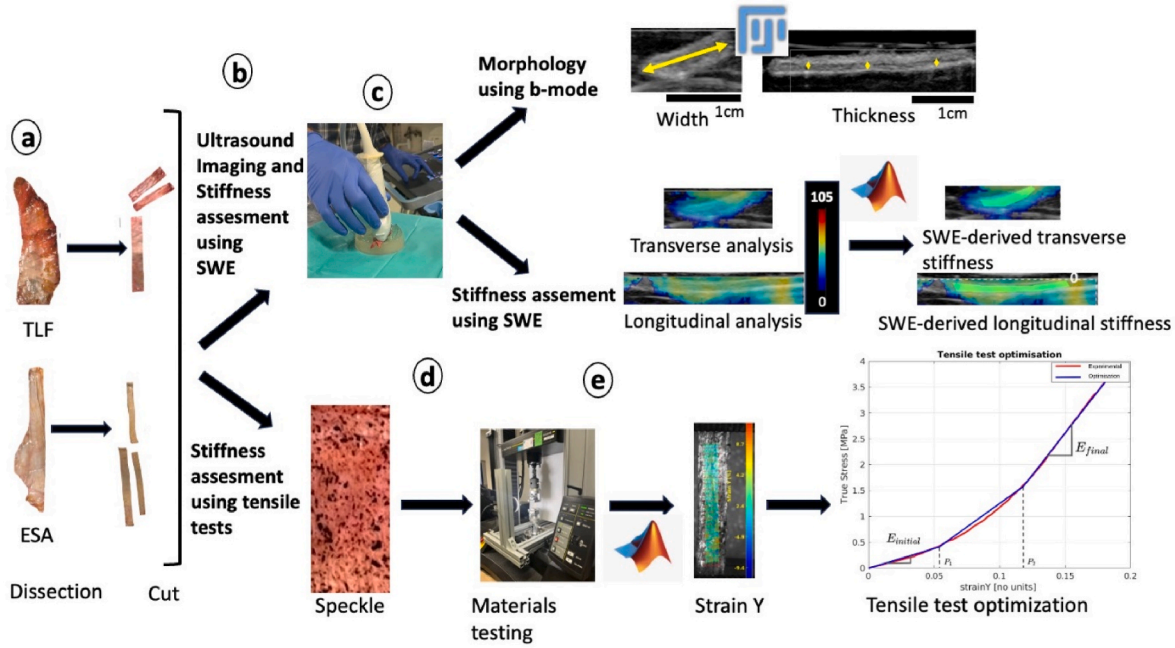

Fig. 2. Provides an overview of the methods used in this study. (a) Firstly, the ThoracoLumbar Fascia (superficial layer) and Erector Spinae Aponeurosis (deep layer) were manually dissected from overlying adipose tissue and underlying muscle, respectively, from 10 fresh human donors. (b) Following this, 60 rectangular samples (approximately 80 mm × 10 mm) were prepared and divided into four groups. TLF samples were taken horizontally and vertically, with their long side aligned with or perpendicular to the direction of the fibers. ESA samples were taken in the axial direction, in either a more cranial or caudal location. (c) The thickness and width of each sample were measured using an Aixplorer® ultrasound scanner. The probe was placed longitudinally for thickness and transversely for width measurement. (c) The shear wave speed (SWS of the thoracolumbar fasciae (TLF) and the erector spinae aponeurosis (ESA) was measured in both longitudinal and transverse directions. (d) Finally, a speckle pattern was applied using China ink and an aerograph. (e) The sample was mounted in an INSTRON testing machine and clamped at both ends. It was then subjected to three consecutive cycles of loading between zero and 5N at a constant speed of 0.5 mm/min, followed by a load to 10 N. The protocol was repeated a second time, following a pause in an unloaded state, by loading the sample to 50 N. (f) The mid-section of the sample was filmed using a high-resolution camera to obtain the local tissue strain with custom Matlab software. (g) The true axial stress was calculated using the thickness and strain measurements. To determine the small and large strain elasticity modulus, an experimental tri-linear curve was fitted by minimizing the mean-square error between the experimental and numerical data.

the samples were sprayed with a physiological saline solution (0.9 % NaCl) during preparation and testing and kept at room temperature (24°). The samples were tested immediately after dissection.

2.3. Morphological measurements

The thickness and width of each sample were measured using an Aixplorer® ultrasound scanner (SuperSonic Imagine, Aix-en-Provence, France) and a linear probe (10–2, SuperSonic Imagine) in 'b-mode'. The sample was placed on a gel pad and covered with a large amount of gel, and the probe was placed longitudinally over, without contact, for thickness measurement (as shown in Fig. 2(c)) and transversely for width measurement. The images were exported and post-processed using ImageJ analysis software (Schindelin et al., 2015).

The thickness of each sample was measured as the distance between the upper and lower hyperechoic structures, as shown by the yellow arrow in Fig. 3(a) below. These structures correspond to non-fibrous tissue that surrounds the fascia and aponeurosis. To account for the spatial variation of thickness, the average of three measurements along the length was calculated for each sample (indicated by the three yellow arrows in Fig. 3(a) below). The width of each sample was measured as the distance between the extremities of the tissue (Fig. 3(b) below). The absence of loose connective tissues eliminates any ambiguity.

2.4. Ultrasound stiffness measurements

The Shear Wave Speed (SWS) of the TLF and the ESA in both the longitudinal and transverse directions was measured using the same ultrasound scanner, probe and protocol. The preset was set to "General" with a transducer frequency of L18-5. Gain was adjusted to M 95 dB, with an opacity setting optimized for elastography visualization. The SWE box dimensions were adjusted to each measurement. The measurement started once the SWS map was stabilized. Three consecutive images were taken of the sample in both the longitudinal axis and in the transverse axis respectively. A custom MATLAB routine, previously developed in our group (Dubois et al., 2015; Vergari et al., 2014), was used to manually define a region of interest (ROI) within the elastogram for each sample. The average value of the *SWS* for each sample was then computed. Furthermore, assuming a constant mass density of 1100 kg/m^3, an average "SWE-derived stiffness" μ was calculated based on the well-established relationship $SWS = \sqrt{\mu/\rho}$, where ρ is the tissue's mass density.

2.5. Mechanical testing

Tensile tests were conducted using a uniaxial setup with a 10 kN load cell (INSTRON® 5566, High Wycombe, England). The TLF and ESA were clamped at each end with self-tightening roller tensile grips. The samples were subjected to uniaxial longitudinal loading. A preload of 1N was applied to remove tissue slack, and the cross-head displacement of the testing system was set to zero. The specimens were preconditioned with five cycles of loading/unloading up to 4 N at a speed of 20 mm/min. Two loading scenarios were employed in this study. Firstly, the specimens were loaded at a constant speed of 0.5 mm/min until a force of 10N was reached. The same protocol was repeated after a pause in an unloaded state, with the sample being loaded to 50N.

Digital image correlation (DIC) was used to measure surface displacement by applying a speckle pattern (China ink sprayed) on the posterior surface of the sample. Images of the sample during deformation were captured using a video camera (resolution 2448x2048; exo264CU3, SVS–Vistek®). Images were acquired at a rate of 1 frame per second. The fascia's field strain distribution was analyzed using a custom MATLAB tissue tracking software developed by Vergari et al. (2016).

The force-displacement data and video camera recordings were manually synchronized using MATLAB. The axial and transverse strain of the region of interest was calculated as the mean of the local strain calculated by DIC. The ultimate strain and strength both were defined as the highest value obtained before the failure of the specimen. Tissue true stress was defined as the ratio of the tensile force measured by the INSTRON to the cross-sectional area, which was calculated as the product of instantaneous tissue width and initial tissue thickness. Instantaneous tissue width was defined as the product of the initial tissue width and the transverse strain measured by DIC.

2.6. Extraction of the infinitesimal stiffness and large-strain modulus using a trilinear curve approximation

A trilinear curve approximation to the experimental true stress-strain curve was performed using the *fmincon* MATLAB function in accordance with the concept illustrated in Fig. 4. In the event of tissue failure, the curve would be truncated at the ultimate tensile strain. Only curves with an r^2 greater than 0.99 were kept. The first linear part of the curve models the small strain mechanical behavior of the tissue. The infinitesimal stiffness ($E_{initial}$) was reported as the slope of the first part of the curve. The second part of the curve was considered to be a transition between small and large strains, and as it was typically non-linear, the slope was not reported. The large-strain stiffness (E_{final}) was reported as the slope of the last part of the curve, which was expected to model the mechanical behavior under large strains.

2.7. Statistical analysis

2.7.1. Statistical difference in mean

The statistical tests were conducted using MATLAB. The changes in stiffness were analyzed according to four variables: 1/**strain magnitude**

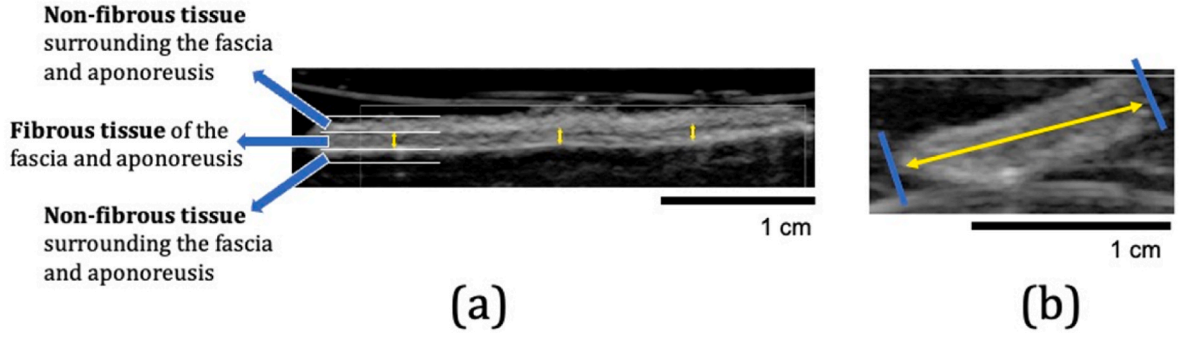

Fig. 3. Ultrasound imaging was used to take morphological measurements. The thickness of each sample was measured as the distance between the upper and lower hyperechoic structures, as shown by the yellow arrow (a). To account for the spatial variation of thickness, we took the average of three measurements along the length for each sample (indicated by the three yellow arrows). The width of each sample was measured as the distance between the extremities of the tissue (b). (For interpretation of the references to color in this figure legend, the reader is referred to the Web version of this article.)

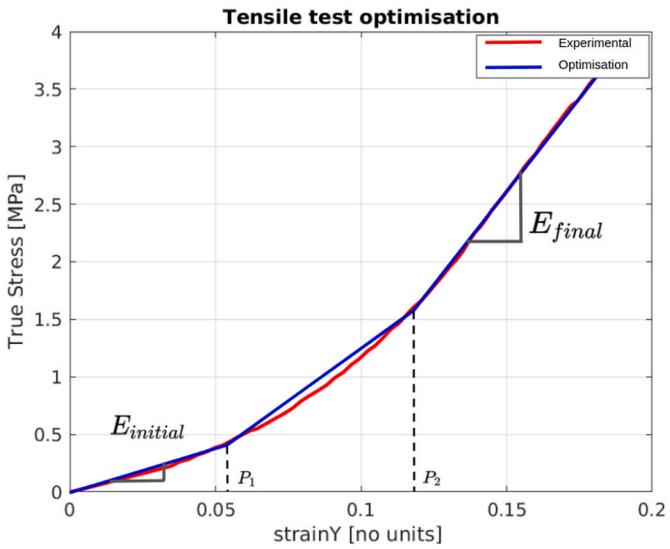

Fig. 4. The true stress-strain curve was divided into three zones using the fmincon MATLAB function for trilinear fitting. The first zone was the small strain zone, from which the infinitesimal stiffness was extracted. The second zone was the transition between small and large strains. The third zone was the large strain zone, from which the large-strain modulus was reported. Only curves with an r^2 greater than 0.99 were kept.

(infinitesimal stiffness versus large-strain stiffness), 2/**loading condition** (10N versus 50 N) and 3/**tissue type** (ESA versus TLF) and 4/the location different locations (ESA CAU, ESA CRA, TLF and Vertebral Aponeurosis).

The normality of the data was first tested using one-sample Kolmogorov-Smirnov test and analyzed with a histogram method. As the variables were not normally distributed, nonparametric tests were used. A **Wilcoxon signed-rank test** was performed to compare the stiffness between 1/the infinitesimal stiffness versus large-strain stiffness 2/for both the 10N loading and 50 N loading conditions and 3/for both tissue type (ESA versus TLF). In the absence of any significant differences between left and right sides, left and right results were pooled. The **Kruskal-Wallis test** and multiple comparisons with the Bonferroni test was used to determine the effect of sample location (ESA CAU, ESA CRA, TLF and VA).

2.7.2. Correlations

The correlation 1/between the infinitesimal stiffness ($E_{initial}$) and the SWE-derived longitudinal and transverse stiffnesses 2/between the large-strain stiffness (E_{final}) and the SWE-derived longitudinal and transverse stiffnesses and 3/infinitesimal stiffness ($E_{initial}$) and the large-strain stiffness (E_{final}) were evaluated. The Pearson correlation coefficient was used in case the data could be assumed normally distributed. If not, the Spearman correlation coefficient was used instead. The normality of the data was assessed with a one-sample Kolmogorov-Smirnov test. A significance level of 0.05 was chosen.

3. Results

3.1. Specimens and qualitative anatomical analysis

A total of $\mathbf{N = 100}$ samples were studied, comprising 24 cranial, 26 caudal, 32 TLF and 18 vertebral aponeurosis. Macroscopically, the TLF was composed of irregularly arranged fibres, with regions of fibrillar rarefaction and even areas devoid of fibres, allowing for the passage of vessels and nerves. The ESA was thick and composed of parallel fibres oriented along the spinal axis. In order to prevent damage to the sample, a small amount of residual muscle or loose connective tissue was left on each sample. The mean thickness of the TLF and of the vertebral aponeurosis was 0.4 mm. The mean thickness of the ESA was 1.1 mm at the cranial level and 1.3 mm at the caudal level.

3.2. Uniaxial tensile test: true stress-strain curves

A total of **152** tensile tests were conducted, with eight samples exhibiting slippage in the grips. In these instances, testing was terminated upon detection of slippage. These samples were subjected to a second round of testing, and the results were incorporated into the subsequent analysis. Fourteen tests were found to be lacking in data, either due to the absence of digital image correlation data or force data. Over the course of the tensile tests, 19 stress-strain curves were deemed unusable. Upon inspection of both the digital images correlation grids and associated strain distributions, a multitude of issues were identified, including light reflection, blurring, insufficient frames, a limited area of strain measurement, shear, and unfolding of the sample under traction.

Ultimately, **119** stress-strain curves were subjected to further analysis. During the testing process, 34 samples reached the ultimate tensile strength. Twenty vertebral aponeuroses reached the ultimate tensile strength during testing. Eleven of these occurred during the 10N loading condition, with a tensile strength ranging from 0.6 to 4.2 MPa (minimum to maximum). Nine occurred during the 50N loading condition, with a tensile strength ranging from 1.9 to 6.6 MPa (minimum to maximum). Nine TLF specimens reached the ultimate tensile strength during the 50N loading condition (tensile strength: 1.6–9 MPa (min-max)). Five ESA cranial specimens reached the ultimate tensile strength.

Fig. 5 presents the experimental true stress-strain curves obtained for $\mathbf{N = 32}$ ThoracoLumbar Fascia (TLF and VA) and $\mathbf{N = 34}$ Erector Spinae Aponeurosis (ESA) samples under the two loading scenarios (maximum loading of 10 N and 50 N) respectively. The stress-strain curves for all tissues exhibited a nonlinear toe region and linear region. The TLF stiffnesses dependence on the fiber direction orientation (longitudinal, transverse) and the ESA stiffnesses dependence on the harvesting region (cranial, caudal) are shown graphically using dashed and dotted lines, respectively.

3.3. Uniaxial tensile test measurements: infinitesimal stiffness and large-strain stiffness

Fig. 6 presents a boxplot illustrating the variation in stiffness, comparing the infinitesimal stiffness for a 10N loading ($E^{10N}_{initial}$), the infinitesimal stiffness for a 50N loading ($E^{50N}_{initial}$), and the large-strain stiffness for a 50N loading (E^{50N}_{final}), based on (a) the laterality of the sample origin (left vs. right), (b) the location of ESA tissue samples (cranial ESA, harvested from top positions, vs. caudal ESA, harvested from bottom positions), and (c) the location of TLF tissue samples (TLF vs. vertebral aponeurosis, VA).

No significant difference was observed due to the laterality of the sample origin (left/right) ($p = 0.495$, $p = 0.764$ and $p = 0.838$ respectively for the initial stiffness values for the 10N loading configuration, initial stiffness values for the 50N loading configuration and the final stiffness values for the 50N loading configuration). Consequently, the data were pooled for the remainder of the analysis.

The null hypothesis, "medians of cranial and caudal ESA are equal" was rejected for the initial stiffness value for the 50N loading configuration with a p-value of 0.029. No significant difference was observed in the initial stiffness values for the 10N loading configuration and the final stiffness values for the 50N loading configuration, with respective p-values of 0.524 and 0.568).

The null hypothesis "medians of TLF and vertebral aponeurosis are equal" was rejected for all the configurations, namely, the infinitesimal stiffness for a 10N loading configuration ($p = 0.006$), the initial stiffness values for the 50N loading configuration ($p = 0.043$) and the final stiffness values for the 50N loading configuration ($p = 0.026$). The

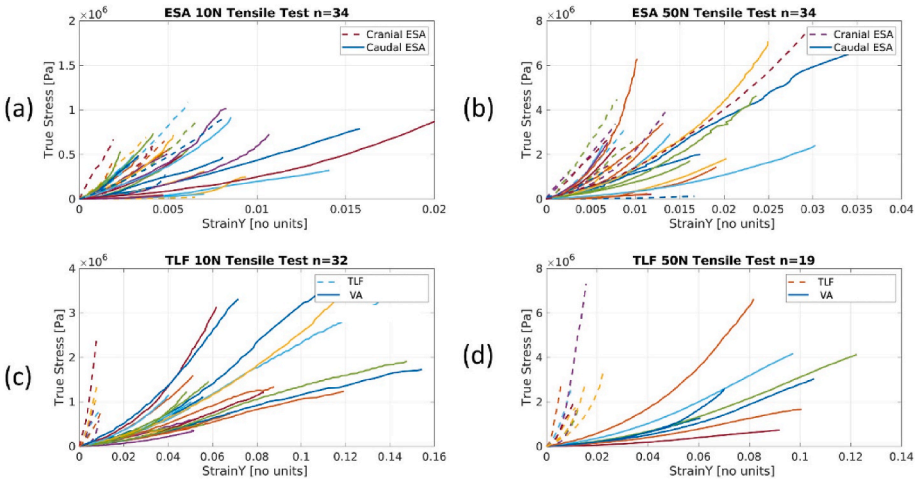

Fig. 5. Experimental true stress-strain curves for the two tissue types and loading conditions. (a, b) Erector Spinae Aponeurosis (ESA) under two different maximum loading conditions: (a) 10N and (b) 50N. Curves are color-coded to distinguish between cranial ESA and caudal ESA samples. (c, d) Thoracolumbar Fascia (TLF) and Vertebral Aponeurosis (VA) under the same loading conditions: (c) 10N and (d) 50N. Curves are color-coded to distinguish between TLF and VA samples. The left column (a, c) corresponds to a maximum applied force of 10N, while the right column (b, d) represents a 50N loading condition. (For interpretation of the references to color in this figure legend, the reader is referred to the Web version of this article.)

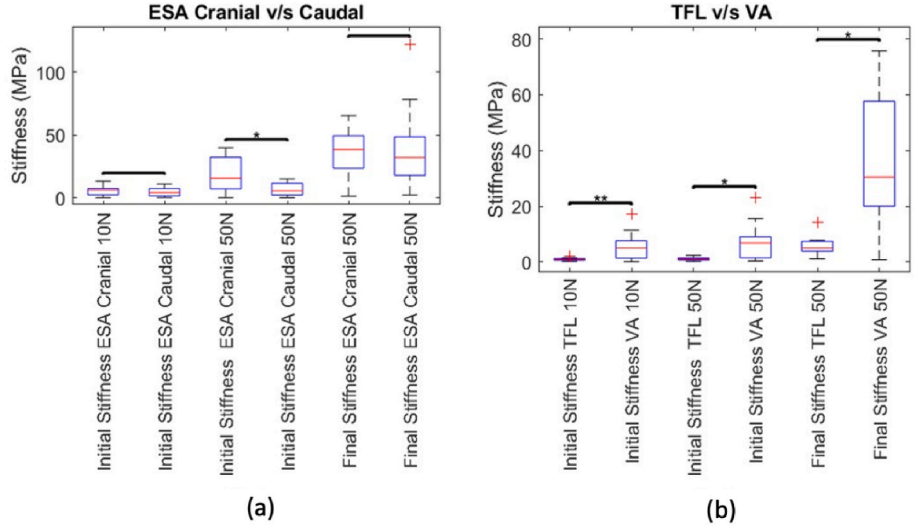

Fig. 6. Boxplot of the stiffness variation for the two loading conditions (10 N versus 50 N) of two variables (a) the location of ESA tissue samples: cranial ESA (ESA harvested from top positions) versus caudal ESA (ESA harvested from bottom positions) and (b) location of TLF tissue sample: TLF (TLF harvested from bottom positions) versus vertebral aponeurosis (VA) (TLF harvested from top positions). Black bars indicate statistical comparisons between groups, and asterisks (*) denote statistically significant differences at $p < 0.05$ (5 % significance level).

associated **median** stiffness demonstrate significant differences between the TLF and the VA: $E^{VA}_{initial} = 0.9$ MPa versus $E^{TLF}_{initial} = 5.0$ MPa for the infinitesimal stiffness for a 10N loading, $E^{VA}_{initial} = 1.2$ MPa versus $E^{TLF}_{initial} = 6.8$ MPa for the infinitesimal stiffness for a 50N loading and $E^{VA}_{final} = 5.0$ MPa versus $E^{TLF}_{final} = 30.5$ MPa for the large-strain stiffness for a 50N loading.

In multiple comparisons with Bonferroni test, the TLF demonstrated a statistically significant difference in the three groups: infinitesimal stiffness for a 10N loading ($E^{10N}_{initial}$), the infinitesimal stiffness for a 50N loading ($E^{50N}_{initial}$), and the large-strain stiffness for a 50N loading (E^{50N}_{final}).

3.4. Correlation between infinitesimal stiffness, SWE-derived longitudinal and transverse stiffness, and large strain stiffness

The correlation between the infinitesimal stiffness of ESA caudal, ESA cranial, TLF and VA (for the pooled data from 10N loading and 50N loading conditions) and the SWE-derived longitudinal and transverse stiffnesses are shown on the scatterplot diagrams in Fig. 7.

There was a negligible to low correlation between the infinitesimal stiffness ($E_{initial}$) and both the SWE-derived longitudinal stiffness (Spearman's rank $r = -0.31$ for cranial ESA, $r = 0.05$ for caudal ESA, $r = 0.09$ for TLF, $r = -0.22$ for VA; $p > 0.05$) and the SWE-derived transverse stiffness (Spearman's rank $r = -0.38$ for cranial ESA, $r = -0.07$ for TLF, $r = -0.31$ for VA; $p > 0.05$). A low negative and significant correlation was identified between initial tensile stiffness and SWE-derived transverse stiffness (Spearman's $r = -0.4$; $p = 0.08$), though its isolated nature limits interpretative relevance.

There was a moderate positive significant correlation (Spearman's rank $r = 0.690$; $p = 10^{-7}$) between the infinitesimal stiffness for a 50N loading ($E^{50N}_{initial}$), and the large-strain stiffness for a 50N loading (E^{50N}_{final}).

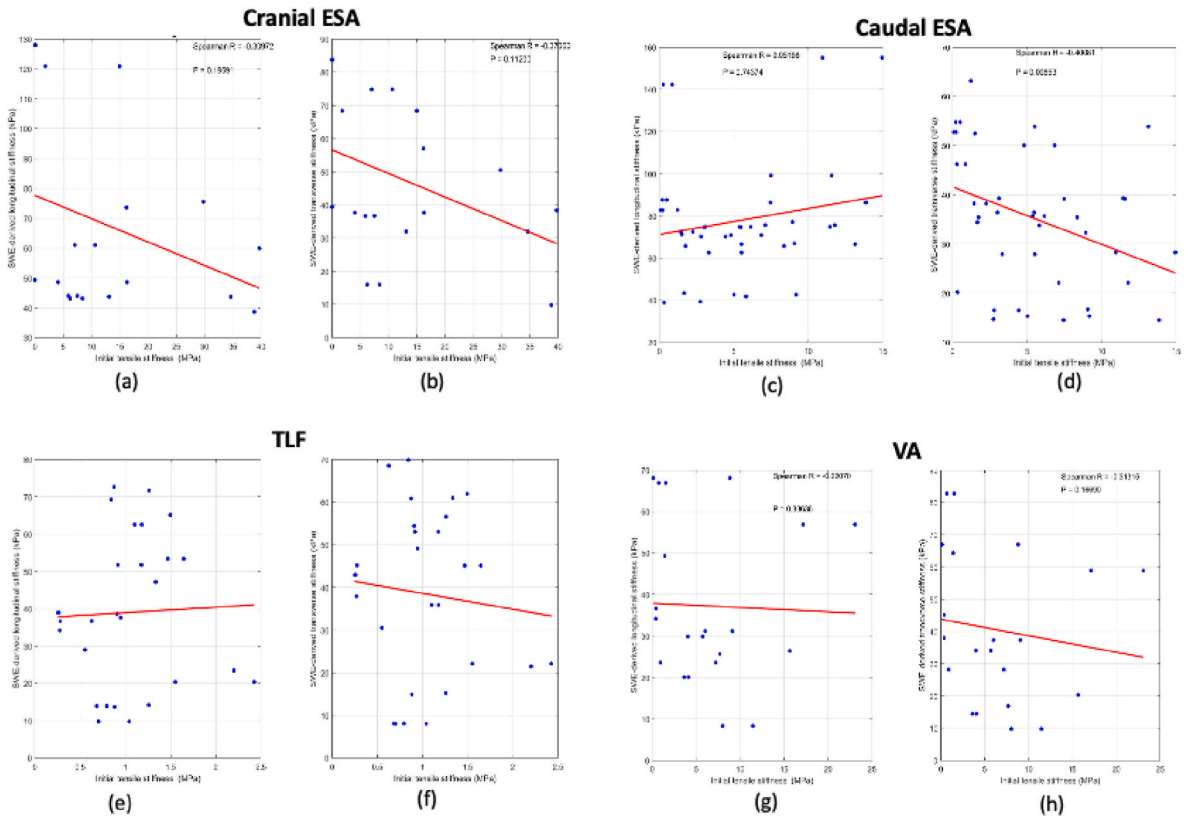

Fig. 7. Scatterplots of the infinitesimal stiffness (pooled data from the 10N loading and 50 N loading conditions respectively) and the SWE-derived longitudinal (a) and transverse (b) stiffnesses of cranial ESA, SWE-derived longitudinal (c) and transverse (d) stiffnesses of caudal ESA, SWE-derived longitudinal (e) and transverse (f) stiffnesses of TLF, and SWE-derived longitudinal (g) and transverse (h) stiffnesses of VA.

Table 1
Comparison of the morphological and mechanical properties in the two tissue types groups and as a function of the fiber direction orientation for the TLF and as a function of the harvesting region (cranial, caudal) for the ESA.

	Cranial ESA median (IQR)	Caudal ESA median (IQR)	TLF median (IQR)	VA median (IQR)
Thickness (mm)	9.0 (0.3)	1.2 (0.3)	0.4 (0.2)	0.4(0.2)
width (mm)	11.5 (2.5)	13.0 (5.3)	17.5 (5.5)	19.0 (8.3)
SWE-derived longitudinal stiffness (kPa)	60.5 (31.6)	74.7 (17.2)	38.2 (33.0)	29.9 (28.4)
SWE-derived transverse stiffness (kPa)	39.0 (36.1)	35.7 (24.1)	43.0 (32.0)	34.1 (42.6)
infinitesimal stiffness 10 N loading (MPa)	6.2 (5.0)	4.1 (5.8)	0.9 (0.6)	5.0 (6.3)
infinitesimal stiffness 50 N loading (MPa)	15.6 (25.1)	5.5 (9.3)	1.2 (0.8)	5.7 (8.0)
large-strain stiffness 50 N (MPa)	38.4 (25.9)	32.0 (30.7)	5.0 (3.5)	30.5 (37.6)

3.5. Comparison of the morphological and mechanical properties

Table 1 below summarizes and compares the morphological and mechanical properties (SWE-derived longitudinal and transverse stiffnesses and the infinitesimal stiffness $E_{initial}$ and large-strain stiffness E_{final}) in the two tissue types groups (TLF and ESA) and as a function of the fiber direction orientation (longitudinal, transverse) for the TLF and as a function of the harvesting region (cranial, caudal) for the ESA. Since most of the distributions did not follow a normal distribution, the results were presented as median and interquartile range (IQR).

4. Discussion

The objective of this study was to characterize the elastic properties of *ex vivo* thoracolumbar fascia (TLF) and erector spinae aponeurosis (ESA) in order to identify differences between the tissues and to explore the potential of SWE for non-invasively characterizing the mechanical properties *in vivo*. This question is significant because the back fasciae and aponeurosis have a major impact on the biomechanics of the spine and may contribute to low back pain. This study presents, for the first time, the measurement of the stiffness of the TLF and ESA separately using uniaxial tensile testing with 2D digital image correlation and shear wave elastography.

The results indicate that there are structural and mechanical differences between the ESA and TLF tissue. The ESA was thicker than TLF and VA, and showed a higher degree of anisotropy. Cranial ESA also tended to be stiffer than the other tissues, and showed higher SWE-derived stiffness. These findings contribute to the understanding of how the back fascia transmits force *in vivo* and can inform future spine models.

With regard to morphological parameters, our study revealed that the fascia thicknesses were found to be lower than those previously reported in the literature. The *ex vivo* thickness measurements reported in the literature ranged from 0.68 to 0.95 mm for the thoracolumbar fascia (TLF) and 1.85 mm for the erector spinae aponeurosis (ESA) (Creze et al., 2018; Benetazzo et al., 2011) Loukas et al. reported a mean thickness of the vertebral aponeurosis of 3 mm (Loukas et al., 2008). US measurements of the TLF ranged from 1.75 mm to 3.7 mm (Devantéry et al., 2023; Larivière et al., 2021; Pirri et al., 2023). These differences may be explained by variations in methodology. The fascia and

aponeurosis are surrounded by loose connective tissue, known as the paratenon, which is transparent and somewhat adherent. The removal of the paratenon to facilitate the use of micrometers and lasers, for instance, may result in damage to the sample. The use of ultrasound analysis enables the identification of the various tissues that comprise the sample, thereby facilitating more accurate measurements.

In the context of the uniaxial tests reported in the literature, it is worth noting that, to the best of our knowledge, the study by Yahia et al. (1993) is the only one to have characterized the biomechanical properties of the TLF of three human body donors. In their study, they assessed the strain-curves load of thin samples with a cross-sectional area of 1 × 1.5 mm and demonstrated that the strains at rupture ranged between 12 % and 15 %. These results have been interpreted by numerous authors as indicating a Stiffness for the TLF in the range of 416–450 MPa, which is more than twice the values obtained in the present study. The methodological approach employed, including sample size and sample number, as well as the manner in which the samples were preserved, are likely to have contributed to these differences. However, it is important to note that these values should be compared to the range of Stiffness values found in the literature. For instance, in the case of thigh and leg muscle fascia (given that no estimations were provided for thoracolumbar fascia (TLF) and erector spinae aponeurosis (ESA)), the Stiffness values range from 100 to 2000 MPa (Bonaldi et al., 2023).

To explore the potential of SWE for non-invasive characterization of mechanical properties *in vivo*, a trilinear curve approximation was used to describe nonlinearity within the tissue. This was preferred over assuming exponential, polynomial, or logarithmic forms of strain energy functions, which have been previously proposed for the well-studied fascia lata (Natali et al., 2010; Pancheri et al., 2014), but never for lumbar fascia. This represents a perspective work. As reported here, the recent study by Wheatley et al. demonstrated differences in stress-strain behaviour between caudal and cranial ESA. The cranial region exhibited a stiffer behaviour than the caudal ESA, which could be attributed to the presence of a more microstructural collagen waviness in the region close to the tendon insertion.

The median SWE-derived stiffness value of the TLF reported in this study falls within the range of results reported by Devantéry et al., 2023 (39.5 ± 18.2 kPa) (Devantéry et al., 2023). Chen et al. reported higher stiffness values ranging from 46.37 ± 0.56 kPa at the L3 level to 52.53 ± 1.05 kPa at the L4 level (Chen et al., 2021). This difference may be explained by the fact that their measurement included both the TLF and the ESA, which has a higher stiffness than that of the TLF. As with the uniaxial test results, we also observed high inter-sample SWE-derived stiffness variations. Lower stiffness was found in the caudal part of the ESA, near the tendon insertion, compared to the cranial part. Additionally, SWE showed higher stiffness in the longitudinal axis of the ESA compared to the transversal axis. The finding may be linked to the orthotropic characteristics of the aponeurosis. This structure has a hierarchical arrangement, similar to that of tendons, with aligned fascicles of collagen-rich fibers and fibrils (Wheatley et al., 2023). Shear waves propagate more quickly along the longitudinal axis of collagen fibers than perpendicular to them (Bouchet et al., 1980). No stiffness difference was found between measurements along the longitudinal and transverse axes in the TLF. This may be due to the interweaving of conjunctive fibers, which gives the tissue an isotropic structure (Bogduk et al., 1984). However, SWE failed to demonstrate the macroscopic anisotropic nature of the vertebral aponeurosis.

As observed in previous studies on the Achilles tendon and the patellar tendon, no correlation was found between the SWE-derived infinitesimal stiffness and the stiffness value measured in tensile testing (Haen et al., 2017; Brandão et al., 2023; Ahmadzadeh et al., 2019). Nevertheless, despite the imprecise absolute values obtained with SWE, they demonstrated the capacity of SWE to quantify relative alterations in human Achilles and patellar tendon stiffness. Our findings are consistent with the low correlation of elasticity values between small-thickness calibrated phantoms measured in SWE (Alrashed et al., 2021; Song et al., 2015). When exploring smaller tissue sizes, there is a tendency to overestimate bias for soft tissue and underestimate bias for hard tissue. This bias occurs because the local homogeneity and the "infinite medium" assumptions for the shear wave equation no longer holds when the tissue size is comparable to the shear wavelength. As a result, the apparent stiffness of the inclusion is biased towards the stiffness of the background material (Li et al., 2019; Sadeghi et al., 2020). Further research is necessary, particularly with regard to the ratio of stress stiffening, which appears to be a more reliable indicator of mechanical behavior than absolute SWE-derived stiffness, given the limitations of SWE in assessing tensile properties in fascial tissues.

Our results align with recent observations regarding the difficulty of linking SWE-measured stiffness with tensile properties in anisotropic tissues. As demonstrated by Götschi et al. (2023), shear wave velocity is influenced by shear viscoelastic properties but does not necessarily reflect tensile stiffness, explaining the absence of correlation between these two parameters in our study. The interpretation of SWE measurements in thin, anisotropic structures remains a challenge. These findings indicate that SWE and tensile testing should be considered complementary rather than interchangeable methods. While tensile testing provides insight into the global response of the tissue under load, SWE may be more useful for assessing local stiffness heterogeneities and variations induced by physiological or pathological conditions. Future research should focus on refining SWE-based modeling approaches to account for anisotropic material properties. One promising direction is the application of acoustoelasticity theory (Gennisson et al., 2007; Bied et al., 2021; Ngo et al., 2024) to quantify third-order elastic parameters, which are directly linked to local stress and could enhance the characterization of fascia tissue mechanics *in vivo*. For instance, Lamb wave and Rayleigh wave-based elastography techniques have been successfully applied to thin or layered tissues, such as the cornea (Nguyen et al., 2011; Tanter et al., 2009), the myocardium (Nenadic et al., 2018), and the bladder (Nenadic et al., 2013), where dispersion analysis accounts for tissue geometry and wave propagation effects. Integrating such methodologies could provide a more comprehensive understanding of the mechanical behavior of fascia and aponeuroses in both healthy and pathological states.

This work is subject to certain limitations. Primarily, the small sample size and the lack of homogeneity of the donor population represent significant constraints. A growing body of evidence indicates a trend towards increased elasticity of fibrous connective tissues, including aponeurosis and tendon, with age (Holt et al., 2016; Shadwick, 1990; Zwirner et al., 2019). It is crucial to acknowledge that the body donors may have been afflicted with lumbar back pathologies, such as osteoarthritis, chronic low back pain, or osteoporotic fractures, which are known to increase with age. Lumbar disease can cause damage, such as increased fascia thickness or biomechanical changes resulting in decreased mobility in perimuscular connective tissue thickness, including the ESA, TLF, and loose connective tissue between them (Langevin, 2011; Langevin et al., 2009; Bishop et al., 2016). Future studies should include a larger number of participants and address younger body donors. Additionally, this work only provides uniaxial data and does not include information on the other axes of the tissue. Previous studies have shown that tissue conditioning, such as freezing, temperature, and hydration, during material testing can influence the tensile properties of the sample. It should also be noted that, in contrast to the tensile tests conducted with preconditioning, the SWS measurements were performed without prior preconditioning of the samples. Given the known nonlinear mechanical behavior of these tissues, as evidenced by the tensile test results, the absence of preconditioning may have influenced the SWE-derived stiffness values. Future studies should investigate the impact of different stretch states and preconditioning protocols on SWE measurements to better characterize the nonlinear elastic response of these anisotropic tissues. All these factors may have contributed to the outcomes observed in this study (Alegre et al., 2016;

Thornton et al., 2001).

A further limitation of this work is that the material testing removes the fascia and aponeurosis from the *in vivo* environment. The study focused on the aponeurosis and TLF of the back, excluding the muscle and superficial fascia. However, it is important to note that these structures are connected by loose connective tissue layers that may contribute to their biomechanics. These layers permit dense connective tissue sheets to glide past one another, which can increase the stiffness of the perimuscular connective tissue and decrease the range of motion. Additionally, the TLF is a large, structurally inhomogeneous fibrous sheet with foramina for vascular pedicle pathways and areas of collagen fibre rarefaction. It can be presumed that this inhomogeneity alters the mechanical behaviour of the fascia and should be considered in a comprehensive study of the fascia. The findings regarding the biomechanical properties of each dense fibrous layer in the back can inform further research.

In summary, the role of the thoracolumbar fascia (TLF) in the pathogenesis of chronic low back pain (CLBP) has received increasing attention in the literature. This study represents a significant breakthrough in that it is the first to determine the stiffness of the erector spinae aponeurosis (ESA) and to reappraise thoracolumbar fascia (TLF) stiffness in human tissue samples *ex vivo*. This advance in understanding spinal biomechanics highlights the critical role of the TLF in conditions such as lumbar pathology and transplantation, as well as its importance in the development of biomechanical spine models and training simulations (Hukins et al., 1990). Furthermore, the research draws attention to the mechanical significance of ESAs, which has previously been overlooked in the literature (McGill, 1987). This paper contributes to clarify the nomenclature and mechanical properties of these tissues based on empirical data, highlighting discrepancies and gaps in the current literature. The study also provides valuable insights into the structural and mechanical differences between ESA and TLF, as well as their respective functions within the spine. Furthermore, the assessment of morphological differences enhances our understanding of these tissues. In particular, the study highlights the limitations of Shear Wave Elastography (SWE) in assessing TLF and emphasizes the importance of caution when interpreting SWE results for TLF assessment. These findings contribute to our understanding of spinal biomechanics and have implications for both research and clinical practice.

CRediT authorship contribution statement

Maud Creze: Writing – original draft, Visualization, Validation, Resources, Project administration, Methodology, Investigation, Funding acquisition, Formal analysis, Data curation, Conceptualization. **Alexandre Lagache:** Writing – original draft, Methodology, Investigation, Formal analysis. **Fabrice Duparc:** Writing – review & editing, Methodology, Investigation, Funding acquisition, Data curation. **Mila Broqué:** Investigation, Formal analysis. **Sylvain Persohn:** Methodology, Investigation, Formal analysis. **Camille Slama:** Investigation. **Claudio Vergari:** Writing – review & editing, Validation, Supervision, Methodology, Investigation, Formal analysis, Data curation. **Pierre-Yves Rohan:** Writing – review & editing, Validation, Supervision, Methodology, Investigation, Formal analysis, Data curation.

Funding

This research did not receive any specific grant from public, commercial, or non-profit funding agencies. However, it was supported by internal resources from ENSAM, Ecole de Chirurgie (Assistance Publique des Hôpitaux de Paris) and Anatomy Laboratory of Rouen University.

Declaration of competing interest

The authors declare that they have no known competing financial interests or personal relationships that could have appeared to influence the work reported in this paper.

Acknowledgements

The authors sincerely thank those who donated their bodies to science so that anatomical research could be performed. Results from such research can potentially increase mankind's overall knowledge that can then improve patient care. The authors are thankful to Mr Bruno Belloncle and to Mr Djamel Taleb for their so valuable technical assistance.

Data availability

Data will be made available on request.

References

Ahmadzadeh, S.M.H., Chen, X., Hagemann, H., Tang, M.-X., , et al.Bull, A.M.J., 2019. Developing and using fast shear wave elastography to quantify physiologically-relevant tendon forces. Med. Eng. Phys. 69, 116–122. https://doi.org/10.1016/j.medengphy.2019.04.005 juill.

Alegre, L.M., Hasler, M., Wenger, S., Nachbauer, W., , et al.Csapo, R., 2016. Does knee joint cooling change in vivo patellar tendon mechanical properties? Eur. J. Appl. Physiol. 116 (10), 1921–1929. https://doi.org/10.1007/s00421-016-3444-5.

Alrashed, A.I., , et al.Alfuraih, A.M., 2021. « reproducibility of shear wave elastography among operators, machines, and probes in an elasticity phantom. Ultrason. Seoul Korea 40 (1), 158–166. https://doi.org/10.14366/usg.20011 janv.

Barker, P.J., Briggs, C.A., , et al.Bogeski, G., 2004. Tensile transmission across the lumbar fasciae in unembalmed cadavers: effects of tension to various muscular attachments. Spine 29 (2), 129–138. https://doi.org/10.1097/01.BRS.0000107005.62513.32 janv.

Barker, P.J., et al., 2006. Effects of tensioning the lumbar fasciae on segmental stiffness during flexion and extension: young investigator award winner. Spine 31 (4), 397–405. https://doi.org/10.1097/01.brs.0000195869.18844.56 févr.

Benetazzo, L., Bizzego, A., De Caro, R., Frigo, G., Guidolin, D., , et al.Stecco, C., 2011. 3D reconstruction of the crural and thoracolumbar fasciae. Surg. Radiol. Anat. SRA 33 (10), 855–862. https://doi.org/10.1007/s00276-010-0757-7.

Bercoff, J., Tanter, M., , et al.Fink, M., 2004. Supersonic shear imaging: a new technique for soft tissue elasticity mapping. IEEE Trans. Ultrason. Ferroelectrics Freq. Control 51 (4), 396–409. https://doi.org/10.1109/TUFFC.2004.1295425 avr.

Berg, W.A., et al., 2012. Shear-wave elastography improves the specificity of breast US: the BE1 multinational study of 939 masses. Radiology 262 (2), 435–449. https://doi.org/10.1148/radiol.11110640 févr.

Bied, M., , et al.Gennisson, J.-L., 2021. Acoustoelasticity in transversely isotropic soft tissues: quantification of muscle nonlinear elasticity. J. Acoust. Soc. Am. 150 (6), 4489. https://doi.org/10.1121/10.0008976.

Bishop, J.H., et al., 2016. Ultrasound evaluation of the combined effects of thoracolumbar fascia injury and movement restriction in a porcine model. PLoS One 11 (1), e0147393. https://doi.org/10.1371/journal.pone.0147393.

Bogduk, N., , et al.Macintosh, J.E., 1984. The applied anatomy of the thoracolumbar fascia. Spine 9 (2), 164–170. https://doi.org/10.1097/00007632-198403000-00006.

Bojairami, I.E., , et al.Driscoll, M., 2022. Coordination between trunk muscles, thoracolumbar fascia, and intra-abdominal pressure toward static spine stability. Spine 47 (9), E423–E431. https://doi.org/10.1097/BRS.0000000000004223 mai.

Bonaldi, L., Berardo, A., Pirri, C., Stecco, C., Carniel, E.L., , et al.Fontanella, C.G., 2023. Mechanical characterization of human fascia lata: uniaxial tensile tests from fresh-frozen cadaver samples and constitutive modelling. Bioengineering 10 (2). https://doi.org/10.3390/bioengineering10020226. Art. n° 2, févr.

Bouchet, P., Gennisson, J.-L., Podda, A., Alilet, M., Carrié, M., , et al.Aubry, S., 1980. Artifacts and technical restrictions in 2D shear wave elastography. Ultraschall Med. Stuttg. Ger. 41 (3), 267–277. https://doi.org/10.1055/a-0805-1099 juin 2020.

Brandão, M. Clara A., Teixeira, G.C., Fontenelle, C. Rubens C., Fontenelle, A., Oliveira, L. F., , et al.Menegaldo, L.L., 2023. Correlation between the shear modulus measured by elastography (SSI) and tangent modulus from tensile tests of in vitro fresh-frozen human tendons. J. Biomech. 160, 111826. https://doi.org/10.1016/j.jbiomech.2023.111826.

Bustami, F.M., 1986. A new description of the lumbar erector spinae muscle in man. J. Anat. 144, 81–91 févr.

Casato, G., Stecco, C., , et al.Busin, R., 2019. Role of fasciae in nonspecific low back pain. Eur. J. Transl. Myol. 29 (3), 8330. https://doi.org/10.4081/ejtm.2019.8330 août.

Chang, J.M., et al., 2011. Clinical application of shear wave elastography (SWE) in the diagnosis of benign and malignant breast diseases. Breast Cancer Res. Treat. 129 (1), 89–97. https://doi.org/10.1007/s10549-011-1627-7 août.

Chen, B., Zhao, H., Liao, L., Zhang, Z., , et al.Liu, C., 2020. Reliability of shear-wave elastography in assessing thoracolumbar fascia elasticity in healthy Male. Sci. Rep. 10 (1), 19952. https://doi.org/10.1038/s41598-020-77123-w.

Chen, B., Liu, C., Lin, M., Deng, W., , et al.Zhang, Z., 2021. Effects of body postures on the shear modulus of thoracolumbar fascia: a shear wave elastography study. Med. Biol. Eng. Comput. 59 (2), 383–390. https://doi.org/10.1007/s11517-021-02320-2 févr.

Creze, M., Soubeyrand, M., Nyangoh Timoh, K., , et al.Gagey, O., 2018. Organization of the fascia and aponeurosis in the lumbar paraspinal compartment. Surg. Radiol. Anat. SRA 40 (11), 1231–1242. https://doi.org/10.1007/s00276-018-2087-0.

Devantéry, K., Morin, M., Grimard, J., , et al.Gaudreault, N., 2023. Effects of a myofascial technique on the stiffness and thickness of the thoracolumbar fascia and lumbar erector spinae muscles in adults with chronic low back pain: a randomized before-and-after experimental study. Bioeng. Basel Switz. 10 (3), 332. https://doi.org/10.3390/bioengineering10030332.

Dorado Cortez, C., Hermitte, L., Ramain, A., Mesmann, C., Lefort, T., , et al.Pialat, J.B., 2016. Ultrasound shear wave velocity in skeletal muscle: a reproducibility study. Diagn. Interv. Imaging 97 (1), 71–79. https://doi.org/10.1016/j.diii.2015.05.010 janv.

Dubois, G., et al., 2015. Reliable protocol for shear wave elastography of lower limb muscles at rest and during passive stretching. Ultrasound Med. Biol. 41 (9), 2284–2291. https://doi.org/10.1016/j.ultrasmedbio.2015.04.020.

Eby, S.F., Song, P., Chen, S., Chen, Q., Greenleaf, J.F., , et al.An, K.-N., 2013. Validation of shear wave elastography in skeletal muscle. J. Biomech. 46 (14), 2381–2387. https://doi.org/10.1016/j.jbiomech.2013.07.033.

Ferraioli, G., et al., 2012. Accuracy of real-time shear wave elastography for assessing liver fibrosis in chronic hepatitis C: a pilot study. Hepatology 56 (6), 2125–2133. https://doi.org/10.1002/hep.25936.

Friedrich-Rust, M., et al., 2008. Performance of transient elastography for the staging of liver fibrosis: a meta-analysis. Gastroenterology 134 (4), 960–974. https://doi.org/10.1053/j.gastro.2008.01.034 e8.

Gennisson, J.-L., et al., 2007. Acoustoelasticity in soft solids: assessment of the nonlinear shear modulus with the acoustic radiation force. J. Acoust. Soc. Am. 122 (6), 3211–3219. https://doi.org/10.1121/1.2793605.

Gennisson, J.-L., Deffieux, T., Fink, M., , et al.Tanter, M., 2013. Ultrasound elastography: principles and techniques. Diagn. Interv. Imaging 94 (5), 487–495. https://doi.org/10.1016/j.diii.2013.01.022 mai.

Götschi, T., Schärer, Y., Gennisson, J.-L., , et al.Snedeker, J.G., 2023. Investigation of the relationship between tensile viscoelasticity and unloaded ultrasound shear wave measurements in ex vivo tendon. J. Biomech. 146, 111411. https://doi.org/10.1016/j.jbiomech.2022.111411.

Gracovetsky, S., Farfan, H.F., , et al.Lamy, C., 1981. The mechanism of the lumbar spine. Spine 6 (3), 249–262. https://doi.org/10.1097/00007632-198105000-00007.

Haen, T.X., Roux, A., Soubeyrand, M., , et al.Laporte, S., 2017. Shear waves elastography for assessment of human achilles tendon's biomechanical properties: an experimental study. J. Mech. Behav. Biomed. Mater. 69, 178–184. https://doi.org/10.1016/j.jmbbm.2017.01.007.

Holt, N.C., Danos, N., Roberts, T.J., , et al.Azizi, E., 2016. Stuck in gear: age-related loss of variable gearing in skeletal muscle. J. Exp. Biol. 219 (Pt 7), 998–1003. https://doi.org/10.1242/jeb.133009 avr.

Hukins, D.W., Aspden, R.M., , et al.Hickey, D.S., 1990. Thorecolumlbar fascia can increase the efficiency of the erector spinae muscles. Clin. Biomech. Bristol Avon 5 (1), 30–34. https://doi.org/10.1016/0268-0033(90)90029-6 févr.

Kirilova, M., Stoytchev, S., Pashkouleva, D., , et al.Kavardzhikov, V., 2011. Experimental study of the mechanical properties of human abdominal fascia. Med. Eng. Phys. 33 (1), 1–6. https://doi.org/10.1016/j.medengphy.2010.07.017 janv.

Langevin, H.M., et al., 2011. Reduced thoracolumbar fascia shear strain in human chronic low back pain. BMC Muscoskelet. Disord. 12, 203. https://doi.org/10.1186/1471-2474-12-203.

Langevin, H.M., et al., 2009. Ultrasound evidence of altered lumbar connective tissue structure in human subjects with chronic low back pain. BMC Muscoskelet. Disord. 10, 151. https://doi.org/10.1186/1471-2474-10-151.

Larivière, C., Henry, S.M., Preuss, et R., 2021. Structural remodeling of the lumbar multifidus, thoracolumbar fascia and lateral abdominal wall perimuscular connective tissues: a search for its potential determinants. J. Anat. 238 (3), 536–550. https://doi.org/10.1111/joa.13330.

Li, G.-Y., Zheng, Y., Jiang, Y.-X., Zhang, Z., , et al.Cao, Y., 2019. Guided wave elastography of layered soft tissues. Acta Biomater. 84, 293–304. https://doi.org/10.1016/j.actbio.2018.12.002 janv.

Lin, P., Chen, M., Liu, B., Wang, S., et, Li, X., 2014. Diagnostic performance of shear wave elastography in the identification of malignant thyroid nodules: a meta-analysis. Eur. Radiol. 24 (11), 2729–2738. https://doi.org/10.1007/s00330-014-3320-9.

Loukas, M., Shoja, M.M., Thurston, T., Jones, V.L., Linganna, S., , et al.Tubbs, R.S., 2008. Anatomy and biomechanics of the vertebral aponeurosis part of the posterior layer of the thoracolumbar fascia. Surg. Radiol. Anat. SRA 30 (2), 125–129. https://doi.org/10.1007/s00276-007-0291-4.

Macintosh, J.E., Bogduk, N., , et al.Gracovetsky, S., 1987. The biomechanics of the thoracolumbar fascia. Clin. Biomech. Bristol Avon 2 (2), 78–83. https://doi.org/10.1016/0268-0033(87)90132-X mai.

McGill, S.M., 1987. A biomechanical perspective of sacro-iliac pain. Clin. Biomech. 2 (3), 145–151. https://doi.org/10.1016/0268-0033(87)90005-2 août.

Natali, A.N., Pavan, P.G., , et al.Stecco, C., 2010. A constitutive model for the mechanical characterization of the plantar fascia. Connect. Tissue Res. 51 (5), 337–346. https://doi.org/10.3109/03008200903389127.

Nelson-Wong, E., Glinka, M., Noguchi, M., Langevin, H., Badger, G.J., , et al.Callaghan, J. P., 2018. Acute surgical injury alters the tensile properties of thoracolumbar fascia in a porcine model. J. Biomech. Eng. 140 (10), 1010121–1010127. https://doi.org/10.1115/1.4040452.

Nenadic, I.Z., et al., 2013. Ultrasound bladder vibrometry method for measuring viscoelasticity of the bladder wall. Phys. Med. Biol. 58 (8), 2675–2695. https://doi.org/10.1088/0031-9155/58/8/2675 avr.

Nenadic, I.Z., Urban, M.W., Pislaru, C., Escobar, D., Vasconcelos, L., , et al.Greenleaf, J. F., 2018. In vivo Open- and closed-chest measurements of left-ventricular myocardial viscoelasticity using lamb wave dispersion ultrasound vibrometry (LDUV): a feasibility study. Biomed. Phys. Eng. Express 4 (4), 047001. https://doi.org/10.1088/2057-1976/aabe41.

Ngo, H.H.P., et al., 2024. Unravelling anisotropic nonlinear shear elasticity in muscles: towards a non-invasive assessment of stress in living organisms. J. Mech. Behav. Biomed. Mater. 150, 106325. https://doi.org/10.1016/j.jmbbm.2023.106325 févr.

Nguyen, Thu-Mai, Couade, M., Bercoff, J., Tanter, et M., 2011. Assessment of viscous and elastic properties of sub-wavelength layered soft tissues using shear wave spectroscopy: theoretical framework and in vitro experimental validation. IEEE Trans. Ultrason. Ferroelectrics Freq. Control 58 (11), 2305–2315. https://doi.org/10.1109/TUFFC.2011.2088.

Otsuka, S., et al., 2018. Site specificity of mechanical and structural properties of human fascia lata and their gender differences: a cadaveric study. J. Biomech. 77, 69–75. https://doi.org/10.1016/j.jbiomech.2018.06.018 août.

Pancheri, F.Q., Eng, C.M., Lieberman, D.E., Biewener, A.A., , et al.Dorfmann, L., 2014. A constitutive description of the anisotropic response of the fascia lata. J. Mech. Behav. Biomed. Mater. 30, 306–323. https://doi.org/10.1016/j.jmbbm.2013.12.002 févr.

Pirri, C., et al., 2023. Ultrasound imaging of thoracolumbar fascia thickness: chronic non-specific lower back pain versus healthy subjects; A sign of a "Frozen Back". Diagn. Basel Switz. 13 (8), 1436. https://doi.org/10.3390/diagnostics13081436 avr.

Qian, Z., et al., 2021. Morphology and mechanical properties of plantar fascia in flexible flatfoot: a noninvasive in vivo study. Front. Bioeng. Biotechnol. 9. Consulté le: 19 janvier 2024. [En ligne]. Disponible sur: https://www.frontiersin.org/articles/10.3389/fbioe.2021.727940.

Ranger, B.J., Moerman, K.M., Feigin, M., Herr, H.M., , et al.Anthony, B.W., 2024. 3D ultrasound shear wave elastography for musculoskeletal tissue assessment under compressive load: a feasibility study. Ultrason. Imag. 46 (4–5), 251–262. https://doi.org/10.1177/01617346241253798.

Sadeghi, S., , et al.Cortes, D.H., 2020. Measurement of the shear modulus in thin-layered tissues using numerical simulations and shear wave elastography. J. Mech. Behav. Biomed. Mater. 102, 103502. https://doi.org/10.1016/j.jmbbm.2019.103502 févr.

Sato, T., Kim, J.H., Cho, K.H., Hayashi, S., Rodríguez-Vázquez, J.F., , et al.Murakami, G., 2021. Fetal development and growth of the human erector spinae with special reference to attachments on the surface aponeurosis. Surg. Radiol. Anat. SRA 43 (9), 1503–1517. https://doi.org/10.1007/s00276-021-02759-w.

Schindelin, J., Rueden, C.T., Hiner, M.C., , et al.Eliceiri, K.W., 2015. The ImageJ ecosystem: an open platform for biomedical image analysis. Mol. Reprod. Dev. 82 (7–8), 518–529. https://doi.org/10.1002/mrd.22489.

Schleip, R., et al., 2012. Strain hardening of fascia: static stretching of dense fibrous connective tissues can induce a temporary stiffness increase accompanied by enhanced matrix hydration. J. Bodyw. Mov. Ther. 16 (1), 94–100. https://doi.org/10.1016/j.jbmt.2011.09.003 janv.

Sebag, F., et al., 2010. Shear wave elastography: a new ultrasound imaging mode for the differential diagnosis of benign and malignant thyroid nodules. J. Clin. Endocrinol. Metab. 95 (12), 5281–5288. https://doi.org/10.1210/jc.2010-0766.

Shadwick, R.E., 1990. Elastic energy storage in tendons: mechanical differences related to function and age. J. Appl. Physiol. Bethesda Md 68 (3), 1033–1040. https://doi.org/10.1152/jappl.1990.68.3.1033, 1985.

Song, P., et al., 2015. Two-dimensional shear-wave elastography on conventional ultrasound scanners with time-aligned sequential tracking (TAST) and comb-push ultrasound shear elastography (CUSE). IEEE Trans. Ultrason. Ferroelectrics Freq. Control 62 (2), 290–302. https://doi.org/10.1109/TUFFC.2014.006628 févr.

Stecco, C., Pavan, P., Pachera, P., De Caro, R., Natali, et A., 2014. Investigation of the mechanical properties of the human crural fascia and their possible clinical implications. Surg. Radiol. Anat. 36 (1), 25–32. https://doi.org/10.1007/s00276-013-1152-y janv.

Tamartash, H., Bahrpeyma, F., , et al.Mokhtari Dizaji, M., 2023. Ultrasound evidence of altered lumbar fascia in patients with low back pain. Clin. Anat. N. Y. N 36 (1), 36–41. https://doi.org/10.1002/ca.23964 janv.

Tanter, M., Touboul, D., Gennisson, J.-L., Bercoff, J., , et al.Fink, M., 2009. High-resolution quantitative imaging of cornea elasticity using supersonic shear imaging. IEEE Trans. Med. Imag. 28 (12), 1881–1893. https://doi.org/10.1109/TMI.2009.2021471.

Thornton, G.M., Shrive, N.G., Frank, et C.B., 2001. Altering ligament water content affects ligament pre-stress and creep behaviour. J. Orthop. Res. Off. Publ. Orthop. Res. Soc. 19 (5), 845–851. https://doi.org/10.1016/S0736-0266(01)00005-5.

Vergari, C., et al., 2014. Intervertebral disc characterization by shear wave elastography: an in vitro preliminary study. Proc. Inst. Mech. Eng. [H] 228 (6), 607–615. https://doi.org/10.1177/0954411914540279 juin.

Vergari, C., Mansfield, J., Meakin, J.R., , et al.Winlove, P.C., 2016. Lamellar and fibre bundle mechanics of the annulus fibrosus in bovine intervertebral disc. Acta Biomater. 37, 14–20. https://doi.org/10.1016/j.actbio.2016.04.002 juin.

Vleeming, A., Pool-Goudzwaard, A.L., Stoeckart, R., van Wingerden, J.P., , et al. Snijders, C.J., 1995. The posterior layer of the thoracolumbar fascia. Its function in load transfer from spine to legs. Spine 20 (7), 753–758 avr.

Wheatley, B.B., Dyer, O.L., Tully, E.E., , et al.Seeley, M.A., 2023. Aponeurosis structure-function properties: evidence of heterogeneity and implications for muscle function. Acta Biomater. 168, 298–308. https://doi.org/10.1016/j.actbio.2023.06.035.

Wilke, J., Schleip, R., Klingler, W., , et al.Stecco, C., 2017. The lumbodorsal fascia as a potential source of low back pain: a narrative review. BioMed Res. Int. 2017, 5349620. https://doi.org/10.1155/2017/5349620.

Willard, F.H., Vleeming, A., Schuenke, M.D., Danneels, L., , et al.Schleip, R., 2012. The thoracolumbar fascia: anatomy, function and clinical considerations. J. Anat. 221 (6), 507–536. https://doi.org/10.1111/j.1469-7580.2012.01511.x.

Xu, W., Zheng, Y., Jiang, Y., Zhang, Z., Ma, S., , et al.Cao, Y., 2023. Shear wave imaging the active constitutive parameters of living muscles. Acta Biomater. 166, 400–408. https://doi.org/10.1016/j.actbio.2023.05.035 août.

Yahia, L.H., Pigeon, P., DesRosiers, et E.A., 1993. Viscoelastic properties of the human lumbodorsal fascia. J. Biomed. Eng. 15 (5), 425–429. https://doi.org/10.1016/0141-5425(93)90081-9.

Yoshitake, Y., Takai, Y., Kanehisa, H., , et al.Shinohara, M., 2014. Muscle shear modulus measured with ultrasound shear-wave elastography across a wide range of contraction intensity. Muscle Nerve 50 (1), 103–113. https://doi.org/10.1002/mus.24104 juill.

Zwirner, J., et al., 2019. Tensile properties of the human iliotibial tract depend on height and weight. Med. Eng. Phys. 69, 85–91. https://doi.org/10.1016/j.medengphy.2019.05.001 juill.